PCCP

PAPER

View Article Online
View Journal | View Issue

Cite this: *Phys. Chem. Chem. Phys.*, 2017, **19**, 18757

Directed assembly of functionalized nanoparticles with amphiphilic diblock copolymers†

Yaru Zhou, Xiaodong Ma, Liangshun Zhang * and Jiaping Lin*

Received 17th May 2017,
Accepted 2nd July 2017

DOI: 10.1039/c7cp03294c

rsc.li/pccp

The ability to design and fabricate highly ordered superstructures from nanoscale particles remains a major scientific and technological challenge. Patchy nanoparticles have recently emerged as a novel class of building units to construct functional materials. Using simulations of coarse-grained molecular dynamics, we propose a simple approach to achieve soft nanoparticles with a self-patchiness nature through self-assembly of tethered copolymers with a sequence of inner solvophilic and outer solvophobic blocks. As building units, the patch-like nanoparticles are directed to further assemble into a rich variety of highly ordered superstructures *via* condensation–coalescence mechanisms. The growth kinetics of the superstructures obeys the kinetic model of the step-growth polymerization process. Our simulations also demonstrate that the intermediate patch-like nanoparticles and the final assembled superstructures can be rationally tuned by changing the number and the composition of the tethered copolymer chains. This strategy of copolymer functionalization conceptually enables the design and fabrication of highly ordered superstructures of nanoparticle ensembles with new horizons for promising applications in soft nanotechnology and biotechnology.

1. Introduction

The current interest in assembling inorganic nanoparticles stems from their collective electronic, optical and magnetic characteristics,[1–4] which are considerably different from those of individual nanoparticles. To date, great progress has been made in controlled assembly of particles into superstructures with desired complexity and functionality according to their vast applications in energy capture and storage, photonics and electronics.[5] Inspired by well-established amphiphilic supramolecular self-assembly,[6–9] the concept of colloidal molecules with solvophilic and solvophobic regions (patches) has been proposed to organize individual particles into particle ensembles. Despite several elegant strategies for the fabrication of micrometer- and submicrometer-sized patchy colloids (*e.g.*, lithography, microfluidics, DNA interactions or glancing angle deposition),[10–18] controlling the number and spatial distribution of patches on the surfaces of nanoscale particles remains a significant challenge in achieving the programmable self-assembly of nanostructured materials.

Recently, functionalization of nanoparticles with a single type of homopolymer has emerged as a simple yet versatile strategy for constructing ever-smaller building units of assembly,[19–30] which are structurally equivalent to amphiphilic diblock copolymers. As a typical example, Kumacheva and co-workers prepared a series of gold nanoparticles functionalized with polystyrene chains,[20] and demonstrated segregation of polymer chains into a number of patches, which are governed by the diameter of the nanoparticles, and the molecular weight and the grafting density of the polymer chains. More importantly, such patchy nanoparticles have the capability to anisotropically assemble into a wide range of superstructures such as trimers and chains. The interparticle distance within the superstructures can be finely adjusted by the physicochemical properties of tethered polymers.

Copolymer functionalization creates additional tuning parameters such as monomer chemistry and block sequence,[31–43] which are significantly different from those of homopolymer functionalization. Due to reconfigurable interfaces of the constituent blocks, the manipulation of flexible copolymer chains nearby the surfaces of nanoparticles offers an effective tool for engineering the interactions of nanoparticles and hence the complexity of the nanoparticle assembly. For instance, He *et al.* used the interfacial ligand-exchange method to covalently tether amphiphilic diblock copolymers onto the surface of gold nanoparticles.[38,39] In selective solvents, the copolymer-functionalized nanoparticles assemble into unimolecular micelles, clusters and

Shanghai Key Laboratory of Advanced Polymeric Materials, State Key Laboratory of Bioreactor Engineering, Key Laboratory for Ultrafine Materials of Ministry of Education, School of Materials Science and Engineering, East China University of Science and Technology, Shanghai, China. E-mail: zhangls@ecust.edu.cn, jlin@ecust.edu.cn

† Electronic supplementary information (ESI) available: Coarse-grained model and simulation method, probability distributions of angle and distance, coordination number of the nanoparticles, the effect of the number of nanoparticles, and effect of the initial configuration of the nanoparticles. See DOI: 10.1039/c7cp03294c

vesicles, depending on the sizes of the polymer chains and nanoparticles. Such structural transitions are distinct from the conventional assembly of amphiphilic diblock copolymers or homopolymer-functionalized particles.

Theoretical and computational research provides valuable microscopic insights into the complex assembly behaviors of copolymer-functionalized nanoparticles.[44–55] In our previous study, a hybrid theory was extended to study the microphase separation of nanoparticles grafted by a single chain of diblock copolymers.[46] Classic structures of diblock copolymers and hierarchically assembled superstructures are formed by regulating the interactions between the nanoparticles and the blocks. Wang and co-workers utilized dissipative particle dynamics to probe the assembly of nanoparticles tethered by amphiphilic diblock copolymers.[54,55] Various hybrid aggregates and nanoparticle organizations were achieved by tuning the interaction parameter between the nanoparticles and the solvophobic blocks. Jayaraman's group utilized computational methods to explore the influence of grafting density, block sequence and particle diameter *etc.* on the assembly behaviors of functionalized nanoparticles in selective solutions or melts of homopolymers.[47–53] These theoretical results enhanced our understanding about the equilibrium nanostructures of functionalized nanoparticles. However, to the best of our knowledge, a study on the microscopic kinetics of the structural evolution of such systems is still lacking. There remains a need for considerable advancements in terms of the structural evolution and the assembly mechanism, which would help experimentalists to construct functional materials with well controllable size and morphologies.

It is worthwhile emphasizing that the experimental and theoretical efforts mainly focus on the case of copolymers with a sequence of inner solvophobic and outer solvophilic blocks. As the block sequence of copolymer molecules is exchanged, the dual nature of the tethered chains makes the compounds particularly sensitive to variations of external conditions and allows the functionalized particles to transition into soft nanoparticles with attractive patches nearby the spherical surfaces.[56–60] As a consequence, such novel systems are able to hierarchically self-assemble first into patch-like nanoparticles and thereafter into complex superstructures. However, the assembled superstructures and the assembly kinetics of such copolymer-functionalized nanoparticles at various levels are still unclear. A deep understanding of superstructures and their formation (*i.e.*, how the arrangement of nanoparticles within the superstructures is tailored by the physicochemical properties of the tethered chains and how the formation and evolution of patch-like nanoparticles are influenced by the specific parameters of the tethered chains) is indispensable to fabricate self-assembling materials satisfying specific application-determined requirements.

In this contribution, we use coarse-grained molecular dynamics to simulate systems of nanoparticles tethered by copolymers with a sequence of inner solvophilic and outer solvophobic blocks, and characterize their hierarchical self-assembly process and their directed assembly configurations as functions of the number and the composition of the tethered copolymer chains. Through tuning the molecular parameters of the copolymer chains, it is possible to control the organization of the nanoparticles within the superstructures of the hybrid systems. Interestingly, we also demonstrate that the molecular parameters of the copolymer chains have a remarkable effect on the assembly kinetics of hierarchical structures at multiple scales. This theoretical work not only offers a novel strategy for controlling the hierarchical self-assembly of nanoparticles, but also demonstrates that the spatial arrangement of nanoparticles within superstructures can be tailored by the molecular design of soft materials.

2. Computational model

We use a coarse-grained representation to model the nanoparticles as hard spheres with diameter D in an implicit solvent. f AB diblock copolymers are uniformly tethered onto the surfaces of nanoparticles, which are schematically illustrated in Fig. 1a. Each copolymer chain consists of A and B blocks with lengths N_A and N_B, respectively. The composition of the diblock copolymers is represented by the volume fraction of B blocks $\alpha = N_B/N$, where $N = N_A + N_B$ is the total length of the copolymer chains. Fig. 1b depicts the interaction potentials for various components. The non-bond interactions between the B

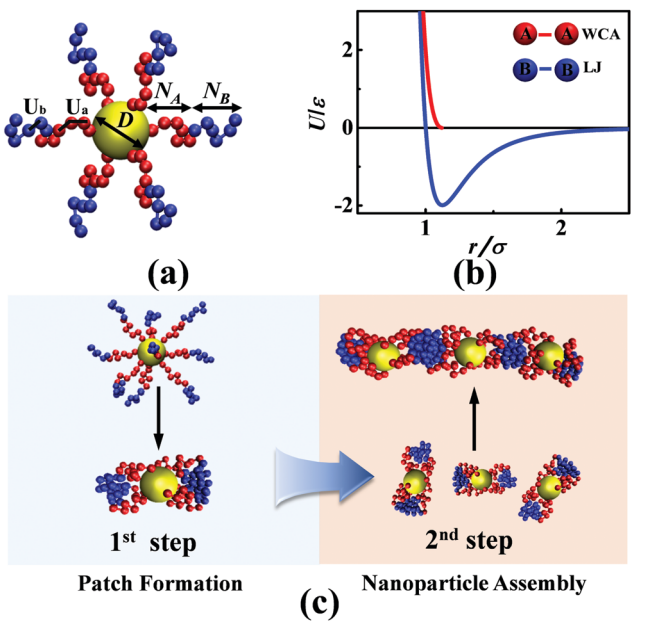

Fig. 1 (a) Schematic representation of nanoparticles decorated by amphiphilic AB diblock copolymers. The diameter of the nanoparticle is denoted by D. The lengths of the inner A block and outer B blocks are represented by N_A and N_B, respectively. U_b and U_a represent the harmonic bond and angle potentials, respectively. (b) Pairwise interaction potentials between various components. The attractive interactions of B–B monomers are modeled *via* the Lennard-Jones (LJ) potential. Other monomers interact through the purely repulsive Weeks–Chandler–Andersen (WCA) potential. (c) Directed assembly of copolymer-functionalized particles *via* the strategy of a stepwise process. 1st step: AB amphiphilic diblock copolymers tethered onto the spherical surfaces self-assemble into patches. 2nd step: the patch-like nanoparticles are directed to assemble into superstructures. Color coding of the components: red (solvophilic A blocks), blue (solvophobic B blocks) and yellow (nanoparticles). The following figures use the same color codes.

monomers are described by the standard 12-6 Lennard-Jones (LJ) potential. The interactions between other pairs of components are treated as the Weeks–Chandler–Andersen (WCA) potential. These settings of interaction potentials imply that the inner A blocks directly tethered onto the surfaces of nanoparticles are solvophilic, while the outer B blocks are solvophobic. Connections of adjacent monomers in the polymer chains are modeled by harmonic potentials (Fig. 1a). To ensure the immobilization of the tethered points, the nanoparticle and the first A monomer of each tethered chain are regarded as rigid bodies. The above systems of copolymer-functionalized nanoparticles are simulated by the Brownian dynamics technique.[61] Each simulation is conducted in the canonical ensemble in a cubical box under periodic boundary conditions and edge length 100σ, where σ is the diameter of the monomers. The integrated time step is fixed at $\Delta t = 0.001\tau$ (τ is the time unit of the simulations). Five separated simulations for given parameter settings are performed to ensure that the observed phenomena are not accidental. All the simulations are carried out with the HOOMD-blue package.[62,63] For more details about the model and method, refer to our previous works and Part A of the ESI.†[64,65]

Although the coarse-grained method used in the molecular dynamics simulations has a significant decrease in the computational cost and accelerates the simulation time, there exist some limitations inherent to the coarse-grained modeling approach on systems of copolymer-functionalized nanoparticles. For example, because a group of neighboring atoms are represented by single beads, a loss of freedom degrees is generated in the coarse-grained mapping, obscuring the chemical details responsible for the functions of the nanoparticles and polymers. Despite these limitations, the coarse-grained models are able to describe an amazing array of complicated systems and predict their fascinating assembly behaviors.[66–69]

3. Results and discussion

Sparked by recent experimental studies of hierarchical self-assembly,[7,8] we theoretically design a stepwise process to direct the assembly of copolymer-functionalized nanoparticles *via* coarse-grained simulations, which is schematically illustrated in Fig. 1c. The assembly involves two crucial steps. In the first step, the incompatibility of the distinct blocks of the copolymer chains drives the occurrence of microphase separation on the isotropic surfaces of the nanoparticles, leading to the formation of anisotropic patch-like particles. Subsequently, such particular nanostructures, as the building units, are directed to further assemble into highly ordered superstructures. To separately elucidate the assembly behaviors of hybrid compounds, this work includes two parts: formation of patch-like nanoparticles and their directed assembly.

3.1 Formation of patch-like nanoparticles

In this subsection, we consider systems of single nanoparticles tethered by amphiphilic AB diblock copolymers. The diameter of the nanoparticles has a value of $D = 4\sigma$. The total length of the copolymer chain is fixed at $N = 12$, but the length of the solvophobic B blocks can be modulated, corresponding to the compositional variation of the tethered chains. Under these parameter settings, the size of the nanoparticles is comparable with the characteristic length of the polymer chains. Below, we concentrate on the effects of the number f and composition α of the tethered chains on the self-assembly behaviors of the amphiphilic AB diblock copolymers.

Fig. 2 illustrates the representative configurations of the amphiphilic AB diblock copolymers tethered onto the spherical surfaces under various combinations of number f and composition α of copolymer chains. The computational time t represented by the time unit τ is annotated on the top of the images. These snapshots sketch a common feature of the structural evolution of diblock copolymers. Initially (at time $t = 0$), the stretched chains are uniformly distributed on the surfaces of the nanoparticles. Subsequently ($t = 10^2\tau$), the solvophobic B blocks (colored in blue) attract each other to form a couple of small patch-like regions, while the solvophilic A blocks (colored in red) remain swollen. To further depress the contribution of energetically unfavorable B block/solvent interfaces, the smaller B-rich regions gradually merge into larger patches due to their dynamic and soft characteristics, simultaneously leading to the strong stretching of the A blocks ($t = 10^3\tau$). Eventually ($t = 10^4\tau$), stable patches of solvophobic B blocks are formed nearby the spherical surfaces, and the solvophilic A blocks are used to establish linkages between the patches and the nanoparticles, as shown in the rightmost snapshots of Fig. 2.

More importantly, from the snapshots of Fig. 2, one can also identify that the valences of the nanoparticles (*i.e.*, the number of patches formed by the solvophobic B blocks) have a tight relation with the molecular design of the tethered chains. Under the parameter settings of number $f = 7$ and composition

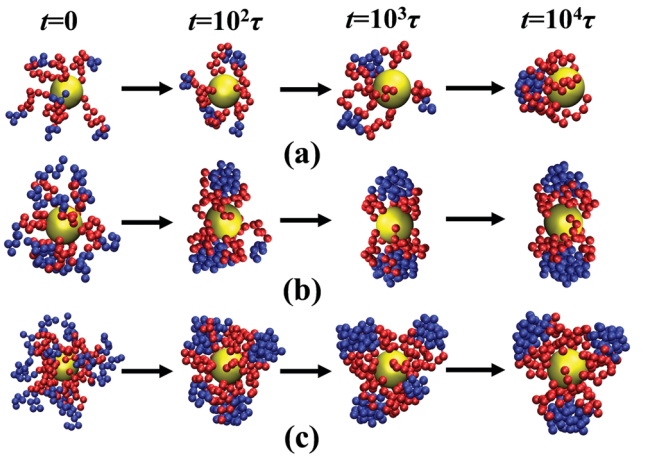

Fig. 2 Representative snapshots of single nanoparticles functionalized with amphiphilic AB diblock copolymers in the course of patch formation under various combinations of number f and composition α of the tethered chains. (a) $f = 7$ and $\alpha = 0.33$, (b) $f = 12$ and $\alpha = 0.50$ and (c) $f = 18$ and $\alpha = 0.50$. The computational time t represented by time unit τ is annotated on the top of the images. The representations of colors are the same as those in Fig. 1.

α = 0.33 of the tethered copolymer chains, the hybrid systems favor the formation of a single solvophobic B patch, because the longer solvophilic A blocks are able to adopt stretchable conformations without a significant amount of entropic loss (Fig. 2a). As the solvophobic B blocks become long, corresponding to the augmentation of the α value, more than one patch is induced by the immobilization feature of the tethered points. For instance, the tethered copolymers with α = 0.5 and f = 12 self-assemble into two separated B patches at the opposite positions of the spheres (Fig. 2b). As the number of tethered chains is increased to 18, segregation of solvophobic B blocks leads to production of three patches uniformly distributed nearby the spherical surface (Fig. 2c).

To systematically capture the effects of the number f and the composition α of the tethered chains on the valences of the nanoparticles, we construct a phase-like diagram of copolymer-functionalized nanoparticles in the f–α parameter space, which is depicted in Fig. 3. The rightmost snapshots highlight the typical self-assembled nanostructures of copolymer-functionalized nanoparticles. We check the equilibration of the simulations by the snapshots of systems at different computational times, and also verify the equilibrium nanostructures through various initial configurations. For the low composition of tethered chains (*e.g.*, $\alpha < 0.25$), the amphiphilic AB diblock copolymers do not have sufficient attractive forces to associate into patch-like structures and remain in an open configuration, even when the number of tethered chains is augmented. In the case of $\alpha > 0.75$, the long solvophobic B blocks collapse into large domains, leading to the production of a compact configuration of polymer chains. In the range of $0.25 \leq \alpha \leq 0.75$, the amphiphilic AB diblock copolymers self-assemble into patches near the spherical surfaces *via* bringing the outer attractive B blocks together and distorting the inner repulsive A blocks. By virtue of the competition between the enthalpic and entropic roles of the polymer chains, the valences of the nanoparticles are tuned by varying the design parameters of the amphiphilic AB diblock copolymers. When the tethered chains are rare and the solvophobic B blocks are short, the copolymers form a single patch near the spherical surfaces. As the number of tethered chains and/or the length of the B blocks becomes large, the copolymers are more entropically favorable to produce two patches. The formation of three patches is achieved by further increasing the number of tethered chains and the length of the B blocks. The above observations indicate that the valences of the patch-like nanoparticles are fully determined by the delicate interplay of the enthalpic/entropic contributions of the flexible polymer chains.

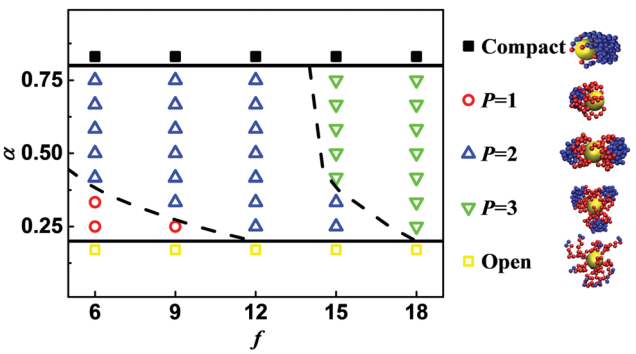

Fig. 3 Phase-like diagram of copolymer-functionalized nanoparticles in terms of the number f and the composition α of the tethered chains. The quantity P stands for the number of patches. Each point corresponds to a simulation result. The solid lines separate the regions of open (or compact) configuration and patches of diblock copolymers. The dashed lines are drawn to separate the boundaries of patches with various numbers. Note that the lines are merely guides to the eyes. Typical configurations of tethered diblock copolymers are shown at the right of the plot.

The molecular design of amphiphilic diblock copolymers not only impacts the valences of the nanoparticles, but also controls the geometrical arrangement of the patches around the nanoparticles. We calculate the angle θ between two patches as well as the distance d between the centers of the patches and the nanoparticles. Fig. S1 of the ESI† depicts the probability distributions of angle and distance for various numbers of tethered chains. As the tethered chains become dense, the nanoparticles with two patches show a narrow distribution of angle with a single peak at roughly $168^\circ \pm 8^\circ$; those with three patches, $120^\circ \pm 13^\circ$. In addition, the patches become close to the spherical surfaces as the number of tethered chains is increased.

The computational results shown in Fig. 2 and 3 suggest that the behaviors of the copolymer-functionalized nanoparticles exhibit a well-defined self-patchiness owing to the characteristic of microphase separation of amphiphilic diblock copolymers tethered onto the curved surfaces. Our simulations also show that the number of patches appears to be straightforwardly dependent upon the number and the composition of the tethered chains, so careful molecular design of the diblock copolymers is necessary to yield soft and dynamic patches with the desired number and spatial distribution. Such particular nanoparticles with anisotropic interactions thereby act as building units for next-level assembly.

3.2 Directed assembly of patch-like nanoparticles

In this subsection, the total number of patch-like nanoparticles is fixed at N = 40. Initially, the patch-like nanoparticles with a given valence are randomly dispersed in a cubical box. In particular, the solvophobic B patches nearby the surfaces of the nanoparticles act as attractive parts, whereas the solvophilic A blocks serve as repulsive parts. We use such anisotropic nanoparticles as building units to explore the formation of ordered superstructures through the specific attachment of solvophobic B patches.

Fig. 4 displays the formation process of complicated superstructures from multiple patch-like nanoparticles. As the solvophilic A blocks are long, the tethered diblock copolymers develop into monovalent Janus-type nanostructures with one solvophilic A-rich region and one solvophobic B patch on opposite sides of the nanoparticles. To further minimize the contribution from the energetically unfavorable B-rich patches, the Janus-type structures undergo the next-level assembly to create dimers of nanoparticles (Fig. 4a). As the assembly time passes, such dimers develop the capability to further attach other nanoparticles, leading to the formation of micelle-like

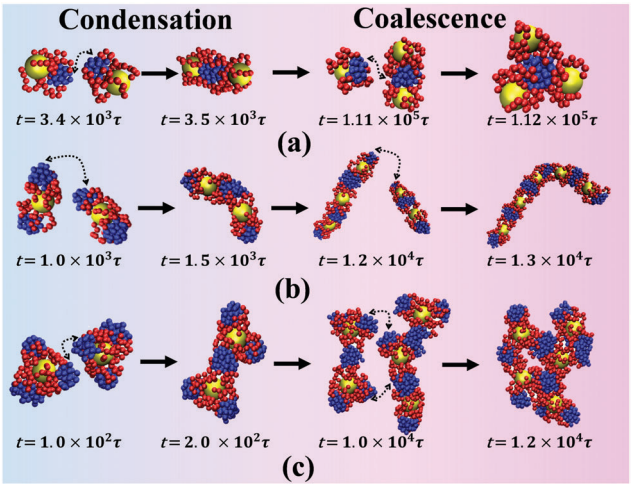

Fig. 4 Representative snapshots of assembled superstructures in the systems of multiple patch-like nanoparticles at a given valence. (a) Monovalent nanoparticles for the number $f = 7$ and the composition $\alpha = 0.33$ of tethered copolymer chains, (b) divalent nanoparticles for $f = 12$ and $\alpha = 0.50$, and (c) trivalent nanoparticles for $f = 18$ and $\alpha = 0.50$. The straight arrows indicate the time sequence. The bent dashed arrows point from the patch to the site where it is going to attach. The background colors are used to distinguish various assembly processes: condensation of free patch-like nanoparticles and coalescence of assembled superstructures.

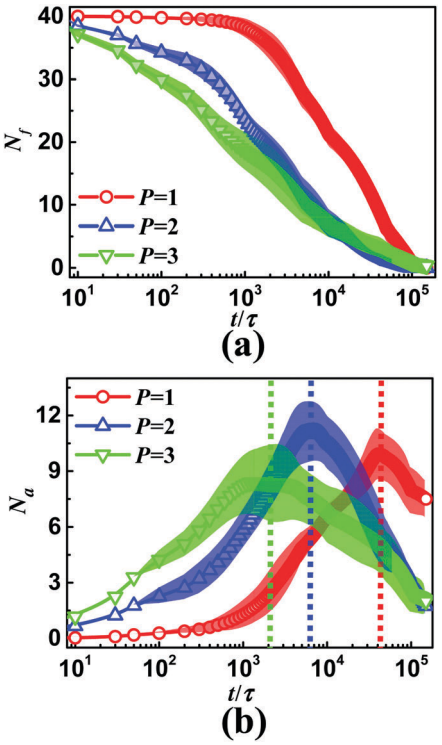

Fig. 5 Assembly kinetics of copolymer-functionalized nanoparticles with a given valence. (a) Number N_f of free nanoparticles and (b) number N_a of assembled superstructures as a function of the computational time. The parameter settings of given valence P for the amphiphilic AB diblock copolymers are the same as those in Fig. 4. The total number of nanoparticles in the simulation boxes is fixed at $N = 40$. The filled areas represent the standard deviations. The vertical dashed lines in image (b) indicate the transitions of assembly mechanisms from the condensation of free nanoparticles to the coalescence of assembled superstructures.

superstructures with a core of solvophobic B blocks and a corona of solvophilic A blocks and nanoparticles. For the copolymer-functionalized nanoparticles with $f = 12$ and $\alpha = 0.5$, the amphiphilic AB diblock copolymers self-assemble into two solvophobic B patches distributed at the opposite poles of the spherical surfaces. Dimers of divalent nanoparticles are quickly formed to alleviate the energetic penalty from the exposed area of solvophobic B patches, yet the 'reactivity' of the non-attached B patches at the ends of the dimers is maintained (Fig. 4b). The dimers of nanoparticles further collide with other isolated superstructures and gradually assemble into oligomers or polymers of nanoparticles, termed as chain-like superstructures. Similarly, the trivalent nanoparticles have a better chance to be connected with each other (Fig. 4c), designated as gel-like superstructures.

From the temporal evolution of superstructures, one can identify that the structural formation of nanoparticles generally involves two distinct processes: condensation of free patch-like nanoparticles and coalescence of assembled superstructures, which are highlighted by the background colors in Fig. 4. During the early stage of assembly, the superstructures grow *via* the condensation of free nanoparticles into dimers, corresponding to the continuous reduction of nanoparticles. As the free nanoparticles get depleted, the formation process of the superstructures shifts from the condensation-governed regime to a period dominated by the coalescence of assembled superstructures.

To better understand the assembly kinetics of copolymer-functionalized nanoparticles, we monitor the number N_f of free nanoparticles and the number N_a of assembled superstructures as a function of the computational time, which are depicted in Fig. 5. For the quantity N_a, only the dimers or the greater aggregations are defined as the superstructures. In the plot of Fig. 5a, the number of free nanoparticles presents a rapid decrease and the valence of patch-like nanoparticles has a pronounced effect on the variation of free nanoparticles. In the plot of Fig. 5b, a maximum value of the number of superstructures emerges, implying the occurrence of distinct assembly mechanisms of nanoparticles. In addition, the position of the maximum value is strongly dependent upon the valences of the patch-like nanoparticles (*i.e.*, the design parameters of the amphiphilic AB diblock copolymers).

These tendencies observed in Fig. 5 can be rationally understood as follows: the assembly kinetics is controlled by the diffusion and the valences of the patch-like nanoparticles. In the initial stage, the free nanoparticles diffuse faster in the solution and more readily find the binding sites, resulting in the rapid reduction of free nanoparticles and the corresponding increase of dimers. It should be pointed out that the trivalent nanoparticles are more likely to find the binding sites, leading to quicker consumption of free nanoparticles and the production of assembled superstructures. As the assembly time passes, the free nanoparticles are gradually depleted and the number of assembled superstructures reaches a maximum value. In the later stage, the assembly mechanism of the functionalized nanoparticles shifts from the condensation of free nanoparticles

to the coalescence of assembled superstructures, which are highlighted by the dashed lines in Fig. 5b. This change gives rise to the consumption of assembled superstructures.

Accumulation of the simulation results from Fig. 4 and 5 suggests that the assembly pathway of patch-like nanoparticles mimics the supracolloidal polymerization (*e.g.*, condensation and coalescence).[70–72] To quantitatively characterize their assembly kinetics, we introduce the number-average degree of polymerization $\bar{x}_n = \sum_x x n_x \Big/ \sum_x n_x$, where x is the number of nanoparticles in the superstructures and n_x is the number of superstructures containing x nanoparticles. Fig. 6 shows the temporal dependence of the number-average degree of polymerization for the divalent patch-like nanoparticles under various numbers of tethered chains. For both cases of chain number $f = 6$ and 12, the number-average degree of polymerization gradually increases as the assembly time passes. Linking with the direct observation of structural evolution (Fig. 4b), one can conclude that the assembly kinetics of the divalent patch-like nanoparticles has the characteristics of step-growth polymerization (SGP) in synthetic polymers.

To provide a definitive confirmation of the SGP process for the assembly of the divalent nanoparticles, we adopt the classic Flory's model of SGP to predict the growth kinetics of the superstructures.[70,73] The relevant equation of the SGP model regarding the kinetic variable is $\bar{x}_n = Kt + 1$, where K is the growth rate of chain-like superstructures. In Fig. 6, the solid lines show the fit curves to the simulation data based on the above mentioned equation. The variation in the average-number degree of polymerization follows a linear relationship in terms of the assembly time, suggesting that the kinetic model of the SGP process properly describes the growth kinetics of the superstructures. Therefore, the formation of chain-like superstructures from the divalent nanoparticles obeys the kinetics of step-growth polymerization.

Next, we consider the effect of amphiphilic diblock copolymers on the final superstructures of hybrid systems and the arrangement of nanoparticles. Fig. 7a–c illustrate the hierarchically assembled superstructures of nanoparticles functionalized with the amphiphilic AB diblock copolymers under various combinations of the number f and composition α of the tethered chains. The insets display the typical configurations of the polymer chains and the arrangement of nanoparticles within the superstructures. Under the condition of a single patch formed by the tethered diblock copolymers with $f = 7$ and $\alpha = 0.33$, the nanoparticles are directed to aggregate into zero-dimensional, micelle-like superstructures (Fig. 7a), where the cores are composed of the solvophobic B blocks and the nanoparticles distribute on the surfaces of the cores. Like the conventional micelles of amphiphilic diblock copolymers only, the assembled superstructures are not uniform in size. Adding a second attraction to the nanoparticles (corresponding to the case of $f = 12$ and $\alpha = 0.50$) encourages the occurrence of aggregation between the various superstructures, because the solvophobic B patches remain at their ends. These linear motifs generate one-dimensional, chain-like superstructures with internal substructures of alternating nanoparticle–polymer sequence, as shown in the inset of Fig. 7b. The dynamic nature of the solvophobic B patches also leads to the formation of branched chains. It should be mentioned that the domain in a repeated unit usually contains one nanoparticle,[55] because of the solvophilic feature of nanoparticles and the repulsions of solvophilic blocks. Adding a third attraction to nanoparticles increases the dimensionality of the assembled superstructures, as illustrated in Fig. 7c. The inset reveals the presence of a highly branched network. Although these superstructures have been observed in the systems of patchy colloids,[70,74–77] this is the first demonstration of

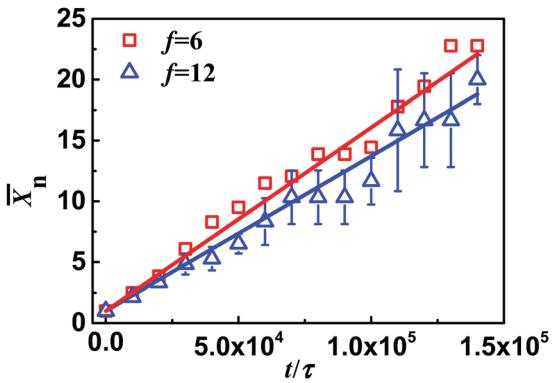

Fig. 6 Temporal dependence of number-average degree of polymerization for divalent patch-like nanoparticles at different numbers of tethered copolymer chains. The solid lines show the relationship $\bar{x}_n = Kt + 1$, where K is the growth rate of chain-like superstructures. The definition of $\bar{x}_n$ is stated in the main text. The composition of the tethered copolymer chains is fixed at $\alpha = 0.5$. For the sake of clarity, the error bars standing for the standard deviations are drawn for the case of $f = 12$.

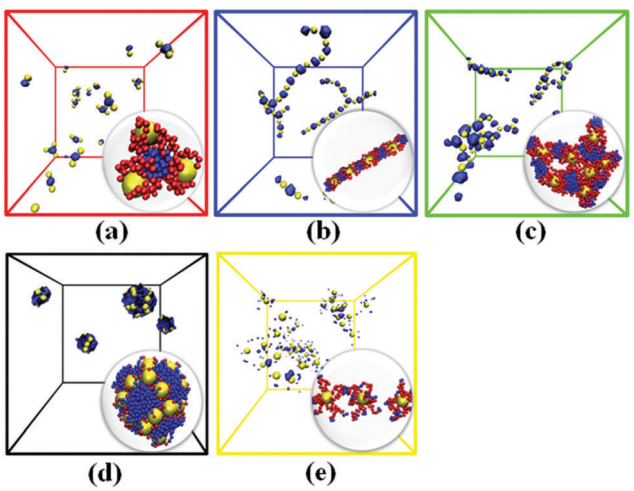

Fig. 7 Typical superstructures of hierarchical assembly of nanoparticles functionalized with amphiphilic AB diblock copolymers. (a) Micelle-like superstructures of nanoparticles with valence $P = 1$ for the number $f = 7$ and the composition $\alpha = 0.33$ of tethered copolymer chains, (b) chain-like superstructures of nanoparticles with valence $P = 2$ for $f = 12$ and $\alpha = 0.50$, (c) gel-like superstructures of nanoparticles with valence $P = 3$ for $f = 18$ and $\alpha = 0.50$, (d) globular nanoparticles for $f = 12$ and $\alpha = 0.92$, and (e) individual nanoparticles for $f = 9$ and $\alpha = 0.17$. For the sake of clarity, the solvophilic A blocks are not drawn. Insets illustrate the configurations of amphiphilic AB diblock copolymers and the arrangement of nanoparticles within the superstructures.

the ability to access all the superstructures using copolymer-functionalized nanoparticles with isotropic surfaces. In other words, the amphiphilic AB diblock copolymers tethered onto the curved surfaces self-assemble into nanopatches with a given valence, and then direct the nanoparticles to hierarchically assemble into hybrid superstructures with a particular arrangement of nanoparticles.

When the composition of the tethered copolymer chains is out of the range of $0.25 \leq \alpha \leq 0.75$, a different scenario of the assembled structures is observed. Once sufficient solvophobic B blocks are exposed in the solvent, aggregation of multiple nanoparticles is the result of strongly attractive forces operating between them. Eventually, this phenomenon leads to a globular configuration of nanoparticles through non-directionally specific forces (Fig. 7d). In the case of $\alpha < 0.25$, strongly repulsive interactions of A blocks make the nanoparticles stable in solution (Fig. 7e). It should be pointed out that the solvophobic B ends of stretchable chains are occasionally merged to form bridges between their tethered points, which are illustrated in the inset of Fig. 7e. The observations from Fig. 7 indiacte that the emergence of self-organized superstructures of copolymer-functionalized nanoparticles is the result of complicated competition between the attractions of the solvophobic B blocks and the repulsions of the solvophilic A blocks.

As anticipated above, the valences of patch-like nanoparticles can be regulated by the molecular design of amphiphilic AB diblock copolymers, *i.e.*, the number f and the composition α of the tethered chains. To clarify their cooperative influence on the superstructures of copolymer-functionalized nanoparticles, a phase-like diagram of superstructures is depicted in Fig. 8. Each point in the diagram corresponds to a computational result and the curves are merely guides to the eyes. For the nanoparticles tethered by the amphiphilic AB diblock copolymers with the composition $\alpha < 0.25$, the individual nanoparticles are distributed in the simulation boxes due to the strong repulsions of long solvophilic A blocks. For the composition $\alpha > 0.75$, the long solvophobic B blocks result in the production of a globular configuration of nanoparticles. In the range of $0.25 \leq \alpha \leq 0.75$, the phase-like diagram is divided into three characteristic zones: micelle-like, chain-like and gel-like superstructures, which are strongly dependent upon the molecular design of amphiphilic AB diblock copolymers. As the values of the number and composition of the tethered chains are small, the copolymer-functionalized nanoparticles are guided to assemble into micelle-like superstructures. Upon increasing the number of tethered chains and/or the length of the solvophobic B blocks, the chain-like arrangement of nanoparticles is observed. The transition from the chain-like to gel-like arrangement of nanoparticles is triggered by continuous increases in the number and/or the composition of the tethered chains. It should be mentioned that the coexistence of superstructures may be observed in the vicinity of phase-like boundaries.

In order to further identify the assembled superstructures of the functionalized nanoparticles, the coordination number of the patch-like nanoparticles is calculated for each parameter setting and its distribution is shown in Fig. S2a of the ESI.†

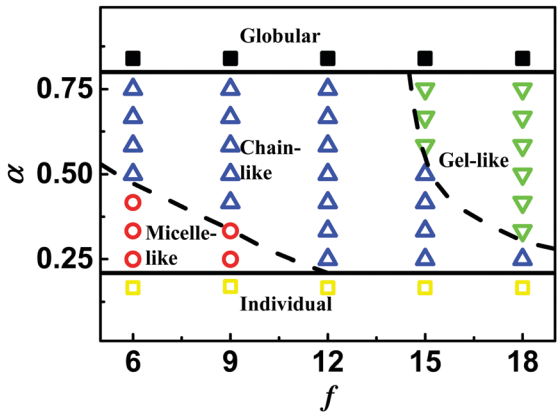

Fig. 8 Phase-like diagram of hierarchically assembled superstructures of nanoparticles functionalized with amphiphilic AB diblock copolymers, plotted in terms of the number f and the composition α of tethered copolymer chains. Each point in the phase-like diagram corresponds to a simulation result. The lines separating the different regions are merely guides to the eyes. By properly tuning the parameters f and α, the copolymer-functionalized nanoparticles are directed to assemble into a number of fascinating ordered superstructures, including micelle-like, chain-like and gel-like superstructures as well as globular and individual nanoparticles.

The average coordination number of the patch-like nanoparticles within the superstructures in terms of the number of tethered copolymer chains is depicted in Fig. S2b of the ESI.† It is demonstrated that the coordination numbers of the nanoparticles within the micelle-like superstructures are close to 3, whereas those within the chain-like superstructures approach 2.

3.3 Discussion

It is instructive to assess the influence of the concentration of copolymer-functionalized nanoparticles on the equilibrium assembled superstructures, which is illustrated in Fig. S3 of ESI.† It is found that the concentration of nanoparticles has a weak effect on the hierarchically assembled superstructures in the regime of relatively dilute solutions and the phase-like diagram in the f–α parameter space (Fig. 8). However, as the concentration of nanoparticles is increased, several defects of joining more than two nanoparticles are produced within the chains, because of the deformability of the soft patches of the solvophobic B blocks.

In Fig. 3 and 8, the boundaries of the phase-like diagram for the structures of single and multiple nanoparticles are similar, implying that the directed assembly of copolymer-functionalized nanoparticles maintains the properties of single nanoparticles such as size, number and arrangement of patches. For instance, the multiple copolymer-functionalized nanoparticles are directed to assemble into chain-like superstructures (Fig. 7b). The average number of patches per nanoparticle within the superstructures has an approximate value of 2, which is consistent with the case of single nanoparticles. Furthermore, under the condition of a relatively dilute solution, the value of the average number of patches is essentially invariant with the concentration of nanoparticles in spite of the existence of branched chains (Fig. S3 of the ESI†).

From the experimental perspective, the self-patchiness behaviors of copolymer-functionalized nanoparticles (originating from the self-assembly of amphiphilic diblock copolymers at the molecular level) play an essential role for practical applications, because it is not necessary to utilize sophisticated facilities and techniques to fabricate the desired patches. Therefore, the copolymer-functionalized nanoparticles appear as a novel class of promising patch-like nanoparticles, which are able to fabricate exotic superstructures of nanoparticles. Looking ahead to possible applications, these highly ordered superstructures (especially the chain-like superstructures with the linear arrangement of nanoparticles) have potential in the fields of medical imaging, biosensing and nanocarriers.

To the best of our knowledge, there are no direct experimental studies on the hierarchical assembly of copolymer-functionalized nanoparticles with the sequence of inner solvophilic and outer solvophobic blocks. Therefore, it is difficult to make direct comparisons between the experimental findings and the computational predictions. However, there still exist some experimental observations regarding the hierarchical assembly of homopolymer-functionalized nanoparticles in the literature to support our computational results. For instance, Kumacheva and co-workers synthesized a series of gold spherical nanoparticles with various diameters,[20] which are grafted by polystyrene chains. Upon changing the solvent conditions, the tethered polymer chains segregate into patchy nanospheres with various valences, which are governed by the length and the grafting density of the polymers. The patchy nanospheres are directed to further assemble into chain-like superstructures *via* the intermediate states of dimers and trimers. In our simulations of coarse-grained molecular dynamics, the copolymer-functionalized nanoparticles first self-assemble into patch-like nanoparticles and thereafter into highly ordered superstructures with various arrangements of nanoparticles (Fig. 2 and 4). Although the computer simulations herein are carried out for the case of amphiphilic diblock copolymers, Fig. 3 and 8 show an analogous behavior that the superstructures of hybrid systems can be tuned by the physicochemical properties of the tethered polymers. In particular, our theoretically proposed systems create additional parameters (such as ratio of solvophobic/solvophilic blocks and sequence of blocks) to regulate the assembled superstructures and the assembly kinetics, which provide a promising route for experimentalists to construct the highly ordered superstructures with tunable spacing and arrangement of nanoparticles.

Beyond reproducing the general features of experiments, our coarse-grained simulations also capture abundant kinetic information of the assembled superstructures, which is currently difficult to be deduced from the experimental observations. For instance, the formation of chain-like superstructures from the divalent nanoparticles obeys the step-growth polymerization (Fig. 6), which is experimentally hypothesized for the assembly kinetics of patchy colloids.[7,8,20] To the best of our knowledge, this is the first example of a clear demonstration of the polymerization kinetics of patch-like nanoparticles *via* computer simulations. Our computational study also provides a clue to link the theory of polymerization reaction in synthetic polymers with the kinetics of supramolecular polymerization at the mesoscopic level.

It should be mentioned that chain-like superstructures can be achieved in systems of copolymer-functionalized nanoparticles with a sequence of inner solvophobic and outer solvophilic blocks.[38,39] Under the condition of low grafting density, strong van der Waals (vdW) forces between proximal functionalized nanoparticles result in the formation of particle chains.[34] In this case, the small spacing between the nanoparticles is determined by competition between the vdW attraction and the steric repulsions. In our current model, the copolymers with the sequence of inner solvophilic and outer solvophobic blocks are adopted. The attractive forces of the outer solvophobic blocks lead to the production of chain-like superstructures. The large spacing between the nanoparticles is principally controlled by the repulsions of the inner solvophilic blocks.

It is worthwhile pointing out that Estridge *et al.* used the coarse-grained model to probe the assembly of copolymer-functionalized nanoparticles,[51] including the formation of patch-like nanoparticles and their assembly structures. The distinct structures at various stages (patches of copolymers at initial stage, chain-like superstructures at intermediate stage and clusters at final stage) are observed. Although our computational model and the simulated results are seemingly similar with their work, the assembled structures of copolymer-functionalized nanoparticles in our work have salient features. Specifically, because of the repulsive interactions of A–A beads, only the B blocks self-assemble into patches and the solvophilic A blocks remain stretchable (Fig. 2). In addition, due to the copolymers with a sequence of inner solvophilic A blocks and the outer solvophobic B blocks, the patch-like nanoparticles are directed to assemble into highly ordered superstructures at the final stage (Fig. 4 and 7), which are strongly dependent upon the valences of the nanoparticles or the molecular parameters of the amphiphilic diblock copolymers.

More importantly, the highly ordered superstructures of copolymer-functionalized nanoparticles originate from the stepwise assembly process in our simulations. As a comparison, we also simulate the formation of superstructures, starting from an initially random configuration of nanoparticles tethered by the stretchable diblock copolymers. The snapshots for the formation of superstructures are displayed in Fig. S4a of the ESI.† In the initial stage of self-assembly, the copolymers tethered onto the spherical surfaces start to form small patches, which are similar to the case shown in Fig. 2. Meanwhile, mutual fusion takes place through random encounters with other copolymer-functionalized nanoparticles. These facts result in the formation of divalent or trivalent patch-like nanoparticles. The subsequent coalescence of oligomers with the trivalent nanoparticles results in the production of a branched arrangement of nanoparticles, which is depicted in Fig. S4b of the ESI.† Similar simulations of systems for the case of monovalent nanoparticles show the coexistence of chain-like and micelle-like architectures,[54] instead of the pure micelle-like superstructures. Comparison with the final configurations of assembled superstructures shown in Fig. 7 suggests that the well-defined superstructures are achieved *via* introduction of a pre-assembly process.

In the current work, the surface patterning of functionalized nanoparticles is mediated by the enthalpic interactions of amphiphilic diblock copolymers. The previous experimental and theoretical results also confirm the fact that the conformational entropy gained from the length mismatch and tethering density of polymer chains is sufficient to obtain patch- or stripe-like nanoparticles.[78–80] Such patterning nanoparticles can also serve as building units to further assemble into a great diversity of fascinating hierarchical architectures, which are similar to the superstructures of copolymer-functionalized nanoparticles. However, the assembly kinetics of such patterning nanoparticles may display salient features. For instance, the formation of hierarchical architectures not only includes the growth mechanisms of condensation and coalescence, but also involves the fragmentation of superstructures owing to the weak interactions between attached patches.[81–83]

4. Conclusions

In summary, we perform simulations of coarse-grained molecular dynamics to demonstrate the hierarchical directed assembly of functionalized nanoparticles by capitalizing on the amphiphilic diblock copolymers, which have the sequence of inner solvophilic and outer solvophobic blocks. In the first step of assembly, the diblock copolymers tethered onto the surfaces of the nanoparticles self-assemble into well-defined patches. The valences of the patch-like nanoparticles can be rationally tuned by changing the number and the composition of the tethered copolymer chains. In the second step, the anisotropic patch-like nanoparticles are guided to assemble into a number of fascinating hybrid superstructures, including micelle-like, chain-like and gel-like superstructures. The formation of superstructures sequentially obeys the following mechanisms: condensation of free patch-like nanoparticles and coalescence of assembled superstructures. The corresponding kinetics has the characteristics of step-growth polymerization. Intriguingly, the assembled superstructures and the assembly kinetics at high level are remarkably affected by the parameters of amphiphilic diblock copolymers at the molecular level.

Acknowledgements

This work was supported by the National Natural Science Foundation of China (21574040 and 21234002), and the Key Laboratory of Advanced Polymer Materials of Shanghai (ZD20170201).

Notes and references

1 Z. Nie, A. Petukhova and E. Kumacheva, *Nat. Nanotechnol.*, 2010, **5**, 15–25.
2 M. R. Jones, K. D. Osberg, R. J. Macfarlane, M. R. Langille and C. A. Mirkin, *Chem. Rev.*, 2011, **111**, 3736–3827.
3 A. Y. Jee, K. Lou, H. S. Jang, K. H. Nagamanasa and S. Granick, *Faraday Discuss.*, 2016, **186**, 11–15.
4 T. Chen, M. Pourmand, A. Feizpour, B. Cushman and B. M. Reinhard, *J. Phys. Chem. Lett.*, 2013, **4**, 2147–2152.
5 M. Grzelczak, J. Vermant, E. M. Furst and L. M. Liz-Marzán, *ACS Nano*, 2010, **4**, 3591–3605.
6 Y. Mai and A. Eisenberg, *Chem. Soc. Rev.*, 2012, **41**, 5969–5985.
7 A. H. Gröschel, F. H. Schacher, H. Schmalz, O. V. Borisov, E. B. Zhulina, A. Walther and A. H. E. Müller, *Nat. Commun.*, 2012, **3**, 710.
8 A. H. Gröschel, A. Walther, T. I. Löbling, F. H. Schacher, H. Schmalz and A. H. E. Müller, *Nature*, 2013, **503**, 247–251.
9 A. H. Gröschel and A. H. E. Müller, *Nanoscale*, 2015, **7**, 11841–11876.
10 A. B. Pawar and I. Kretzschmar, *Macromol. Rapid Commun.*, 2010, **31**, 150–168.
11 A. B. Pawar and I. Kretzschmar, *Langmuir*, 2008, **24**, 355–358.
12 Y. Wang, Y. Wang, D. R. Breed, V. N. Manoharan, L. Feng, A. D. Hollingsworth, M. Weck and D. J. Pine, *Nature*, 2012, **491**, 51–56.
13 S. C. Glotzer and M. J. Solomon, *Nat. Mater.*, 2007, **6**, 557–562.
14 L. Feng, R. Dreyfus, R. Sha, N. C. Seeman and P. M. Chaikin, *Adv. Mater.*, 2013, **25**, 2779–2783.
15 Y. Ke, L. L. Ong, W. M. Shih and P. Yin, *Science*, 2012, **338**, 1177–1183.
16 N. Hijnen and P. S. Clegg, *Langmuir*, 2014, **30**, 5763–5770.
17 F. Li, D. P. Josephson and A. Stein, *Angew. Chem., Int. Ed.*, 2011, **50**, 360–388.
18 E. Duguet, A. Désert, A. Perro and S. Ravaine, *Chem. Soc. Rev.*, 2011, **40**, 941–960.
19 R. M. Choueiri, A. Klinkova, H. Thérien-Aubin, M. Rubinstein and E. Kumacheva, *J. Am. Chem. Soc.*, 2013, **135**, 10262–10265.
20 R. M. Choueiri, E. Galati, H. Thérien-Aubin, A. Klinkova, E. M. Larin, A. Querejeta-Fernández, L. Han, H. L. Xin, O. Gang, E. B. Zhulina, M. Robinstein and E. Kumacheva, *Nature*, 2016, **538**, 79–83.
21 B. Gao, M. J. Rozin and A. R. Tao, *Nanoscale*, 2013, **5**, 5677–5691.
22 B. Bozorgui, D. Meng, S. K. Kumar, C. Chakravarty and A. Cacciuto, *Nano Lett.*, 2013, **13**, 2732–2737.
23 A. Chremos and A. Z. Panagiotopoulos, *Phys. Rev. Lett.*, 2011, **107**, 105503.
24 P. Akcora, H. Liu, S. K. Kumar, J. Moll, Y. Li, B. C. Benicewicz, L. S. Schadler, D. Acehin, A. Z. Panagiotopoulos, V. Pryamitsyn, V. Ganesan, J. Ilavsky, P. Thiyagarajan, R. H. Colby and J. F. Douglas, *Nat. Mater.*, 2009, **8**, 354–359.
25 J. Choi, C. M. Hui, M. Schmitt, J. Pietrasik, S. Margel, K. Matyjazsewski and M. R. Bockstaller, *Langmuir*, 2013, **29**, 6452–6459.
26 A. Chremos and J. F. Douglas, *Soft Matter*, 2016, **12**, 9527–9537.
27 H.-Y. Lee, S. H. R. Shin, A. M. Drews, A. M. Chirsan, S. A. Lewis and K. J. M. Bishop, *ACS Nano*, 2014, **8**, 9979–9987.
28 S. H. R. Shin, H.-Y. Lee and K. J. M. Bishop, *Angew. Chem., Int. Ed.*, 2015, **54**, 10816–10820.
29 C.-K. Wu, K. L. Hultman, S. O'Brien and J. T. Koberstein, *J. Am. Chem. Soc.*, 2008, **130**, 3516–3520.
30 C. Yi, S. Zhang, K. T. Webb and Z. Nie, *Acc. Chem. Res.*, 2017, **50**, 12–21.

31 J. Song, G. Niu and X. Chen, *Bioconjugate Chem.*, 2017, **28**, 105–114.
32 Y. Liu, Y. Liu, J.-J. Yin and Z. Nie, *Macromol. Rapid Commun.*, 2015, **36**, 711–725.
33 Y. Liu, J. He, K. Yang, C. Yi, Y. Liu, L. Nie, N. M. Khashab, X. Chen and Z. Nie, *Angew. Chem., Int. Ed.*, 2015, **54**, 15809–15812.
34 K. J. M. Bishop, *Angew. Chem., Int. Ed.*, 2016, **55**, 1598–1600.
35 X. Qian, J. Li and S. Nie, *J. Am. Chem. Soc.*, 2009, **131**, 7540–7541.
36 Z. Posel, P. Posocco, M. Fermeglia, M. Lisal and S. Pricl, *Soft Matter*, 2013, **9**, 2936–2946.
37 Z. Posel, P. Posocco, M. Lísal, M. Fermeglia and S. Pricl, *Soft Matter*, 2016, **12**, 3600–3611.
38 J. He, Y. Liu, T. Babu, Z. Wei and Z. Nie, *J. Am. Chem. Soc.*, 2012, **134**, 11342–11345.
39 J. He, X. Huang, Y.-C. Li, Y. Liu, T. Babu, M. A. Aronova, S. Wang, Z. Lu, X. Chen and Z. Nie, *J. Am. Chem. Soc.*, 2013, **135**, 7974–7984.
40 X. Yu, S. Zhong, X. Li, Y. Tu, S. Yang, R. M. Van Horn, C. Ni, D. J. Pochan, R. P. Quirk, C. Wesdemiotis, W.-B. Zhang and S. Z. D. Cheng, *J. Am. Chem. Soc.*, 2010, **132**, 16741–16744.
41 J. Song, L. Cheng, A. Liu, J. Yin, M. Kuang and H. Duan, *J. Am. Chem. Soc.*, 2011, **133**, 10760–10763.
42 X. Yu, W.-B. Zhang, K. Yue, X. Li, H. Liu, Y. Xin, C.-L. Wang, C. Wesdemiotis and S. Z. D. Cheng, *J. Am. Chem. Soc.*, 2012, **134**, 7780–7787.
43 B. Ni, M. Huang, Z. Chen, Y. Chen, C.-H. Hsu, Y. Li, D. Pochan, W.-B. Zhang, S. Z. D. Cheng and X.-H. Dong, *J. Am. Chem. Soc.*, 2015, **137**, 1392–1395.
44 J. R. Spaeth, I. G. Kevrekidis and A. Z. Panagiotopoulos, *J. Chem. Phys.*, 2011, **135**, 184903.
45 B. Vorselaars, J. U. Kim, T. L. Chantawansri, G. H. Fredrickson and M. W. Matsen, *Soft Matter*, 2011, **7**, 5128–5137.
46 X. Zhu, L. Wang, J. Lin and L. Zhang, *ACS Nano*, 2010, **4**, 4979–4988.
47 N. Nair and A. Jayaraman, *Macromolecules*, 2010, **43**, 8251–8263.
48 A. Seifpour, P. Spicer, N. Nair and A. Jayaraman, *J. Chem. Phys.*, 2010, **132**, 164901.
49 T. B. Martin, A. Seifpour and A. Jayaraman, *Soft Matter*, 2011, **7**, 5952–5964.
50 T. B. Martin, C. McKinney and A. Jayaraman, *Soft Matter*, 2013, **9**, 155–169.
51 C. E. Estridge and A. Jayaraman, *J. Chem. Phys.*, 2014, **140**, 144905.
52 C. E. Estridge and A. Jayaraman, *J. Polym. Sci., Part B: Polym. Phys.*, 2015, **53**, 76–88.
53 C. E. Estridge and A. Jayaraman, *ACS Macro Lett.*, 2015, **4**, 155–159.
54 S. Ma, Y. Hu and R. Wang, *Macromolecules*, 2015, **48**, 3112–3120.
55 S. Ma, Y. Hu and R. Wang, *Macromolecules*, 2016, **49**, 3535–3541.
56 B. Capone, I. Coluzza, F. LoVerso, C. N. Likos and R. Blaak, *Phys. Rev. Lett.*, 2012, **109**, 238301.
57 B. Capone, I. Coluzza, R. Blaak, F. LoVerso and C. N. Likos, *New J. Phys.*, 2013, **15**, 095002.
58 E. Bianchi, B. Capone, G. Kahl and C. N. Likos, *Faraday Discuss.*, 2015, **181**, 123–138.
59 C. Koch, A. Z. Panagiotopoulos, F. Lo Verso and C. N. Likos, *Soft Matter*, 2015, **11**, 3530–3535.
60 L. Rovigatti, B. Capone and C. N. Likos, *Nanoscale*, 2016, **8**, 3288–3295.
61 D. Frenkel and B. Smit, *Understanding Molecular Simulation: From Algorithms to Applications*, Academic Press, San Diego, CA, 2nd edn, 2002.
62 J. A. Anderson, C. D. Lorenz and A. Travesset, *J. Comput. Phys.*, 2008, **227**, 5342–5359.
63 J. Glaser, T. D. Nguyen, J. A. Anderson, P. Lui, F. Spiga, J. A. Millan, D. C. Morse and S. C. Glotzer, *Comput. Phys. Commun.*, 2015, **192**, 97–107.
64 Y. Li, S. Lin, X. He, J. Lin and T. Jiang, *J. Chem. Phys.*, 2011, **135**, 014102.
65 C. Cai, Y. Li, J. Lin, L. Wang, S. Lin, X.-S. Wang and T. Jiang, *Angew. Chem., Int. Ed.*, 2013, **52**, 7732–7736.
66 Z. Zhang, M. A. Horsch, M. H. Lamm and S. C. Glozter, *Nano Lett.*, 2003, **3**, 1341–1346.
67 Z. Zhang and S. C. Glotzer, *Nano Lett.*, 2004, **4**, 1407–1413.
68 G. Srinivas and J. W. Pitera, *Nano Lett.*, 2008, **8**, 611–618.
69 J. Zhang, Z.-Y. Lu and Z.-Y. Sun, *Soft Matter*, 2013, **9**, 1947–1954.
70 Q. Chen, J. K. Whitmer, S. Jiang, S. C. Bae, E. Luijten and S. Granick, *Science*, 2011, **331**, 199–202.
71 K. Liu, Z. H. Nie, N. N. Zhao, W. Li, M. Rubinstein and E. Kumacheva, *Science*, 2010, **329**, 197–200.
72 R. Guo, J. Mao, X.-M. Xie and L.-T. Yan, *Sci. Rep.*, 2014, **4**, 7021.
73 P. J. Flory, *Principles of Polymer Chemistry*, Cornell University Press, New York, 1953.
74 Q. Chen, S. C. Bae and S. Granick, *Nature*, 2011, **469**, 381–384.
75 Q. Chen, J. Yan, J. Zhang, S. C. Bae and S. Granick, *Langmuir*, 2012, **28**, 13555–13561.
76 Z.-W. Li, Z.-Y. Lu, Y.-L. Zhu, Z.-Y. Sun and L.-J. An, *RSC Adv.*, 2013, **3**, 813–822.
77 Z.-W. Li, Z.-Y. Lu, Z.-Y. Sun and L.-J. An, *Soft Matter*, 2012, **8**, 6693–6697.
78 G. A. DeVries, M. Brunnbauer, Y. Hu, A. M. Jackson, B. Long, B. T. Neltner, O. Uzun, B. H. Wunsch and F. Stellacci, *Science*, 2007, **315**, 358–361.
79 C. Singh, P. K. Ghorai, M. A. Horsch, A. M. Jackson, R. G. Larson, F. Stellacci and S. C. Glotzer, *Phys. Rev. Lett.*, 2007, **99**, 226106.
80 Z. Liu, R. Guo, G. Xu, Z. Huang and L. T. Yan, *Nano Lett.*, 2014, **14**, 6910–6916.
81 I. A. Nyrkova and A. N. Semenov, *Macromol. Theory Simul.*, 2005, **14**, 569–585.
82 T. P. J. Knowles, C. A. Waudby, G. L. Devlin, S. I. A. Cohen, A. Aguzzi, M. Vendruscolo, E. M. Terentjev, M. E. Welland and C. M. Dobson, *Science*, 2009, **326**, 1533–1537.
83 A. J. Markvoort, H. M. M. ten Eikelder, P. A. J. Hilbers and T. F. A. de Greef, *ACS Cent. Sci.*, 2016, **2**, 232–241.

